

Marchenko imaging below an overburden with random scatterers

Kees Wapenaar, Jan Thorbecke, Joost van der Neut, Ivan Vasconcelos and Evert Slob

summary

Marchenko imaging is a new way to deal with internal multiple scattering in migration. It has been designed for layered media with smooth interfaces. Here we analyze the performance of the Marchenko scheme for a medium with many point scatterers. Although the conditions for Marchenko imaging are violated, we observe from a numerical experiment that the signal-to-noise ratio of the obtained image is significantly higher than with standard imaging.

Introduction

Marchenko imaging has recently been introduced as a new way to deal with internal multiple scattering in migration (Broggini and Snieder, 2012; Wapenaar et al., 2013, 2014; Broggini et al., 2014; Slob et al., 2014; Behura et al., 2014). The method makes use of focusing functions that account for internal multiple scattering. To derive these functions from reflection data at the surface, it is assumed that they are separated in time from the Green's functions. In 1-D media this assumption is strictly valid. In 2-D and 3-D media this assumption is obeyed at limited offsets in layered media with smooth interfaces (Wapenaar et al., 2013). The examples in the aforementioned references obey these conditions. In media with a random distribution of point scatterers, the focusing function and Green's function partly overlap in time, meaning that the conditions for the current Marchenko imaging methodology are not fulfilled. In a companion paper, van der Neut et al. (2014) analyse in detail how the Marchenko scheme handles a small number of isolated point scatterers. Here we apply the Marchenko scheme to a medium with many point scatterers. From both analyses it follows that, although the conditions for Marchenko imaging are violated, the method performs reasonably well (and significantly better than standard migration).

Marchenko method for layered media with smooth interfaces

The Marchenko method is based on the following two Green's function representations (Wapenaar et al., 2014; Slob et al., 2014)

$$\overbrace{G^{p,+}(\mathbf{x}_0'', \mathbf{x}_i', t)}^{t > t_d(\mathbf{x}_0'', \mathbf{x}_i')} + \overbrace{f_1^-(\mathbf{x}_0'', \mathbf{x}_i', t)}^{t < t_d(\mathbf{x}_0'', \mathbf{x}_i')} = \int_{\partial\mathbb{D}_0} d\mathbf{x}_0 \int_{-\infty}^t R(\mathbf{x}_0'', \mathbf{x}_0, t-t') f_1^+(\mathbf{x}_0, \mathbf{x}_i', t') dt' \quad (1)$$

and

$$\overbrace{G^{p,-}(\mathbf{x}_0'', \mathbf{x}_i', t)}^{t \geq t_d(\mathbf{x}_0'', \mathbf{x}_i')} - \overbrace{f_1^+(\mathbf{x}_0'', \mathbf{x}_i', -t)}^{t \leq t_d(\mathbf{x}_0'', \mathbf{x}_i')} = - \int_{\partial\mathbb{D}_0} d\mathbf{x}_0 \int_{-\infty}^t R(\mathbf{x}_0'', \mathbf{x}_0, t-t') f_1^-(\mathbf{x}_0, \mathbf{x}_i', -t') dt', \quad (2)$$

respectively. We explain these representations at the hand of Figures 1 and 2. First note that in our notation \mathbf{x}_0 stands for variable \mathbf{x} at the surface $x_3 = x_{3,0} = 0$ and \mathbf{x}_i is a variable \mathbf{x} at depth level $\partial\mathbb{D}_i$ (here at $x_3 = x_{3,i} = 1100$ m). Starting on the right in equation (1) we have the focusing function $f_1^+(\mathbf{x}_0, \mathbf{x}_i', t)$.

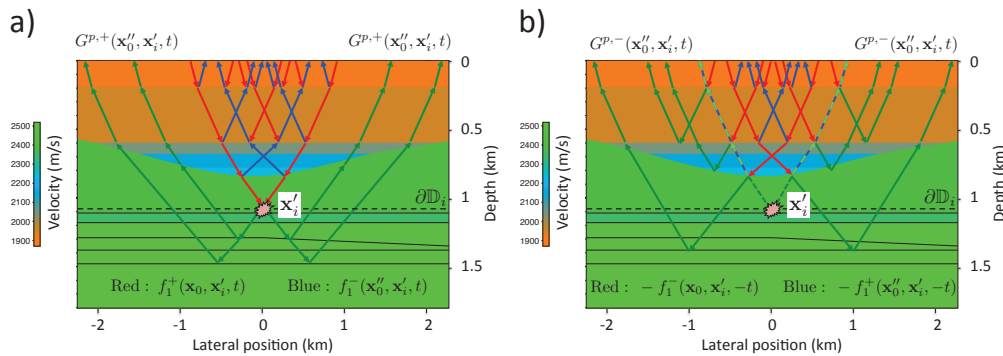


Figure 1 Physical interpretation of equations (1) and (2). (a) The incident field $f_1^+(\mathbf{x}_0, \mathbf{x}_i', t)$ focuses at \mathbf{x}_i' (red rays). Its response consists of $f_1^-(\mathbf{x}_0'', \mathbf{x}_i', t)$ (blue rays) and the Green's function $G^{p,+}(\mathbf{x}_0'', \mathbf{x}_i', t)$ (green rays). (b) The incident field $-f_1^-(\mathbf{x}_0, \mathbf{x}_i', -t)$ (red rays) gives rise to $-f_1^+(\mathbf{x}_0'', \mathbf{x}_i', -t)$ (blue rays) and the Green's function $G^{p,-}(\mathbf{x}_0'', \mathbf{x}_i', t)$ (green rays).

This is a downgoing wave field which, when emitted from the surface into the medium, focuses at \mathbf{x}_i' at $t = 0$ (denoted by the red rays in Figure 1a). When internal multiples could be ignored, $f_1^+(\mathbf{x}_0, \mathbf{x}_i', t)$ would be defined as the time-reversal of the direct arrival of the Green's function, $G_d(\mathbf{x}_0, \mathbf{x}_i', t)$, similar as in e.g. the CFP method (Berkhout and Verschuur, 2001). However, when multiples can not be ignored, the focusing function $f_1^+(\mathbf{x}_0, \mathbf{x}_i', t)$ contains a complex coda that compensates for the internal multiples during propagation from the surface to the focal point. The right-hand side of equation (1) describes the reflection response of the medium to $f_1^+(\mathbf{x}_0, \mathbf{x}_i', t)$. According to the left-hand side, this response consists

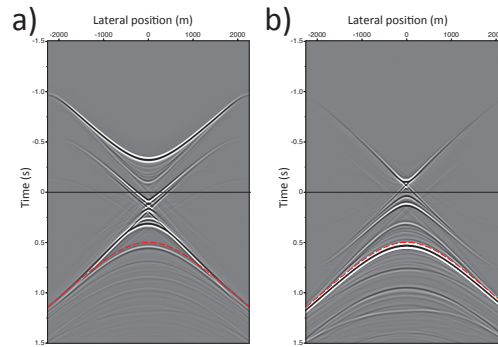


Figure 2 (a) The reflection response of the inhomogeneous medium to $f_1^+(\mathbf{x}_0, \mathbf{x}'_i, t)$ (equation 1). (b) The reflection response of the medium to $-f_1^-(\mathbf{x}_0, \mathbf{x}'_i, -t)$ (equation 2). The red curves separate the focusing functions [$t < t_d(\mathbf{x}''_0, \mathbf{x}'_i)$] from the Green's functions [$t > t_d(\mathbf{x}''_0, \mathbf{x}'_i)$].

of two parts. Because $f_1^+(\mathbf{x}_0, \mathbf{x}'_i, t)$ focuses at \mathbf{x}'_i , this point acts as a virtual source for downgoing waves, so a part of the response is the Green's function $G^{p,+}(\mathbf{x}''_0, \mathbf{x}'_i, t)$. Here the second superscript (+) refers to the source for downgoing waves at \mathbf{x}'_i and the first superscript (p) refers to the observed quantity (acoustic pressure) at \mathbf{x}''_0 . This Green's function is represented by the green rays in Figure 1a. Because of causality, this Green's function exists only for $t > t_d(\mathbf{x}''_0, \mathbf{x}'_i)$, where $t_d(\mathbf{x}''_0, \mathbf{x}'_i)$ is the direct arrival time. The other part of the reflection response to $f_1^+(\mathbf{x}_0, \mathbf{x}'_i, t)$ is the upgoing part of the focusing function, $f_1^-(\mathbf{x}''_0, \mathbf{x}'_i, t)$ (denoted by the blue rays in Figure 1a), which exists only for $t < t_d(\mathbf{x}''_0, \mathbf{x}'_i)$. The total response, i.e., the complete left-hand side of equation (1), is shown in Figure 2a. The red line denotes the direct arrival time $t_d(\mathbf{x}''_0, \mathbf{x}'_i)$. Equation (2) is explained in a similar way by Figures 1b and 2b. Keep in mind that time-reversal changes the propagation direction. Hence, the upgoing blue rays in Figure 1a are replaced by downgoing red rays in Figure 1b, and vice versa.

Because for layered media with smooth interfaces the focusing functions and the Green's functions are well separated in time (see equations (1) and (2) as well as Figure 2), they can be retrieved from the reflection response $R(\mathbf{x}''_0, \mathbf{x}_0, t)$. The procedure is as follows. First, consider equations (1) and (2) for $t < t_d(\mathbf{x}''_0, \mathbf{x}'_i)$. For this time interval the Green's functions on the left-hand sides are zero, hence, we are left with two equations for the two unknowns $f_1^+(\mathbf{x}_0, \mathbf{x}'_i, t)$ and $f_1^-(\mathbf{x}_0, \mathbf{x}'_i, t)$. To avoid the trivial solution, $f_1^+(\mathbf{x}_0, \mathbf{x}'_i, t)$ is written as $f_1^+(\mathbf{x}_0, \mathbf{x}'_i, t) = G_d(\mathbf{x}_0, \mathbf{x}'_i, -t) + M^+(\mathbf{x}_0, \mathbf{x}'_i, t)$, where $M^+(\mathbf{x}_0, \mathbf{x}'_i, t)$ is the coda. Assuming an estimate of the direct arrival of the Green's function is available, the system of equations is solved for $M^+(\mathbf{x}_0, \mathbf{x}'_i, t)$ and $f_1^-(\mathbf{x}_0, \mathbf{x}'_i, t)$. Once these are found, they are substituted into equations (1) and (2), which are now evaluated for $t \geq t_d(\mathbf{x}''_0, \mathbf{x}'_i)$ to obtain $G^{p,+}(\mathbf{x}''_0, \mathbf{x}'_i, t)$ and $G^{p,-}(\mathbf{x}''_0, \mathbf{x}'_i, t)$.

Application of the Marchenko method to a medium with random scatterers

The temporal separation of focusing functions and Green's functions, as illustrated in Figure 2, breaks down when the medium contains point scatterers, because several diffraction hyperbolae of the focusing function cross the direct arrival time $t_d(\mathbf{x}''_0, \mathbf{x}'_i)$ of the Green's function, see van der Neut et al. (2014) for an analysis. The Marchenko method discussed above is not designed to deal with overlapping focusing and Green's functions. We nevertheless apply it to a configuration with many scatterers and evaluate its performance. Figure 3a shows a configuration with an overburden containing many strong point scatterers, and a target zone (the region below $\partial\mathbb{D}_i$) with three weak scatterers, indicated by the red ellipse. The background medium is homogeneous, with a propagation velocity of 1900 m/s. A shot record $R(\mathbf{x}''_0, \mathbf{x}_0, t)$, with its source \mathbf{x}_0 at the central position at the surface, is shown in Figure 3b. A time-dependent gain of $\exp(0.6 * t)$ has been applied to emphasize the multiple scattering. We define the direct arrival of the Green's function, $G_d(\mathbf{x}_0, \mathbf{x}'_i, t)$, as the wave field propagating through the homogeneous background from the indicated virtual source point at \mathbf{x}'_i to all \mathbf{x}_0 at the surface. Using the reflection data at the surface and the time-reversal of this direct Green's function, we solve equations (1) and (2), following the procedure discussed above. The retrieved functions on the left-hand sides of these

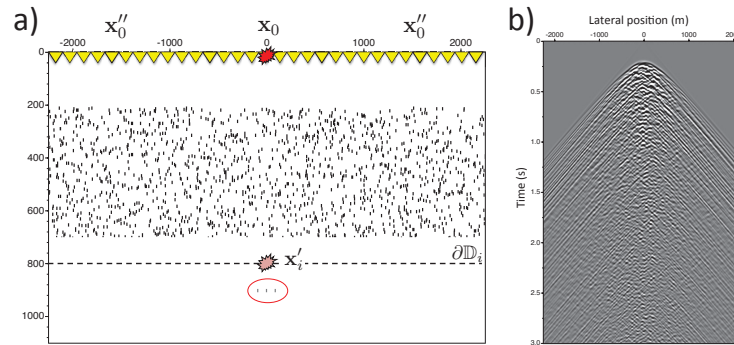


Figure 3 (a) Model, with an overburden with strong random scatterers and a target with three weak scatterers. (b) Reflection response $R(\mathbf{x}_0'', \mathbf{x}_0'', t)$.

equations are shown in Figure 4, in which we used $t_d(\mathbf{x}_0'', \mathbf{x}_i')$ to separate the focusing functions from the Green's functions. Note that the mute at $t_d(\mathbf{x}_0'', \mathbf{x}_i')$ looks quite artificial, particularly in Figures 4a and 4b, since the curve $t_d(\mathbf{x}_0'', \mathbf{x}_i')$ cuts through diffraction hyperbolae (van der Neut et al., 2014). Moreover, compared with Figure 2, the functions in Figure 4 look very noisy because of the many scatterers. Nevertheless, we will show that the 'noise' in these figures contains relevant information about the point scatterers in the target zone.

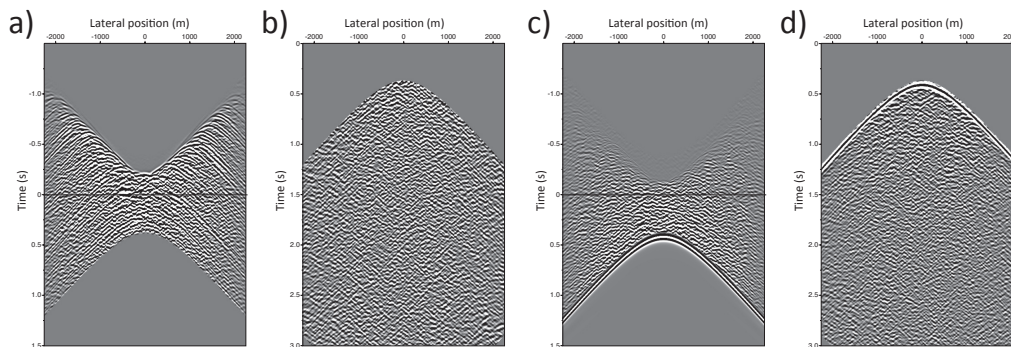


Figure 4 Results of Marchenko scheme, applied to the reflection response of the model in Figure 3. Like in Figure 2, the left-hand sides of equations (1) and (2) are shown, but separated into focusing functions and Green's functions. (a) $f_1^-(\mathbf{x}_0'', \mathbf{x}_i', t)$. (b) $G^{p,+}(\mathbf{x}_0'', \mathbf{x}_i', t)$. (c) $-f_1^+(\mathbf{x}_0'', \mathbf{x}_i', -t)$. (d) $G^{p,-}(\mathbf{x}_0'', \mathbf{x}_i', t)$.

To this end, we use the retrieved Green's functions to image the target zone. First, by repeating the whole procedure for many virtual-source positions \mathbf{x}_i' at $\partial\mathbb{D}_i$, we obtain many Green's functions $G^{p,+}(\mathbf{x}_0'', \mathbf{x}_i', t)$ and $G^{p,-}(\mathbf{x}_0'', \mathbf{x}_i', t)$. Using source-receiver reciprocity, we obtain $G^{-q}(\mathbf{x}_i', \mathbf{x}_0'', t)$ and $G^{+q}(\mathbf{x}_i', \mathbf{x}_0'', t)$, with volume injection-rate sources (q) at all \mathbf{x}_0'' at the surface, and receivers for upgoing ($-$) and downgoing ($+$) waves at all \mathbf{x}_i' at $\partial\mathbb{D}_i$. The reflection response of the target zone, $R(\mathbf{x}_i, \mathbf{x}_i', t)$, can be resolved from $G^{-q}(\mathbf{x}_i, \mathbf{x}_0'', t) = \int_{\partial\mathbb{D}_i} R(\mathbf{x}_i, \mathbf{x}_i', t) * G^{+q}(\mathbf{x}_i', \mathbf{x}_0'', t) d\mathbf{x}_i'$ by multidimensional deconvolution (the asterisk stands for temporal convolution). Subsequently, we use $R(\mathbf{x}_i, \mathbf{x}_i', t)$ to image the target zone. The result is shown in Figure 5a. Note that the three point diffractors are very well imaged and that the noise related to the multiple scattering in the overburden is weak. For comparison, Figure 5b shows the result of standard imaging, applied to the reflection response $R(\mathbf{x}_0'', \mathbf{x}_0'', t)$ at the surface. Here the signal-to-noise ratio is significantly lower.

Conclusion and discussion

Although Marchenko imaging has been designed for layered media with smooth interfaces, we have tested its performance in a medium with random scatterers. From our numerical experiment we observe that the signal-to-noise ratio is significantly higher with Marchenko imaging than with standard imaging. Further improvements can be expected if the separation between focusing functions and Green's

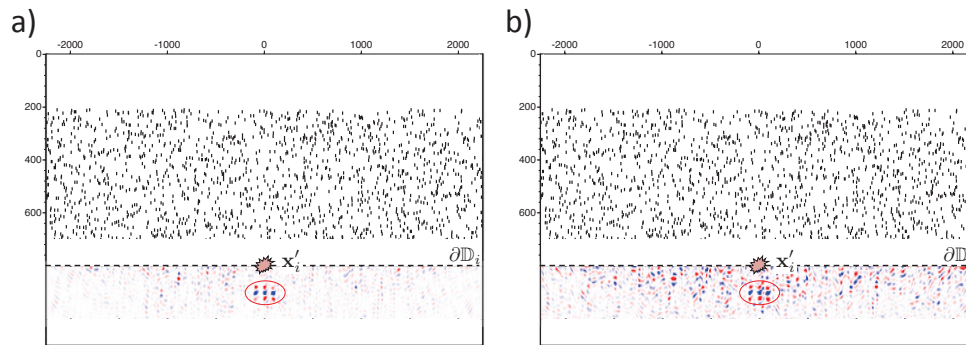


Figure 5 (a) Result of Marchenko imaging, applied to the target zone. (b) Result of standard imaging.

functions is applied in a more sophisticated way, as mentioned by van der Neut et al. (2014).

An interesting aspect of Marchenko imaging, when compared with full waveform inversion (Virieux and Operto, 2009) or full wavefield migration (Berkhout and Verschuur, 2011), is that the target zone can be imaged without the need to image the complex distribution of scatterers in the overburden first.

Another aspect is spatial resolution. For comparable random-scatterer configurations, Fink (2008) and Garnier and Papanicolaou (2014) show that the scatterers enlarge the effective aperture angle and hence improve the spatial resolution. The difference with our configuration is that Garnier and Papanicolaou (2014) use real receivers below the overburden (comparable with the virtual-source method of Bakulin and Calvert (2006)), whereas Fink (2008) backpropagates the transmission response of real sources through the real medium. Hence, both methods make use of the measured transmission response of the scattering medium. The analysis of van der Neut et al. (2014) leads to the conclusion that a scattering overburden does not help to improve the spatial resolution properties of the current Marchenko imaging scheme. This is confirmed by the example in Figure 5. Keep in mind, though, that Marchenko imaging only uses reflection data at the surface and the direct arrivals of the background medium, but no measurements of the complex transmission response. Hence, Marchenko imaging addresses a significantly more difficult problem.

References

- Bakulin, A. and Calvert, R. [2006] The virtual source method: Theory and case study. *Geophysics*, **71**(4), SI139–SI150.
- Behura, J., Snieder, R. and Wapenaar, K. [2014] Autofocus imaging: Image reconstruction based on inverse scattering theory. *Geophysics*, **79**, (accepted).
- Berkhout, A.J. and Verschuur, D.J. [2001] Seismic imaging beyond depth migration. *Geophysics*, **66**, 1895–1912.
- Berkhout, A.J. and Verschuur, D.J. [2011] Full wavefield migration, utilizing surface and internal multiple scattering. *SEG, Expanded Abstracts*, 3212–3216.
- Broggini, F. and Snieder, R. [2012] Connection of scattering principles: a visual and mathematical tour. *European Journal of Physics*, **33**, 593–613.
- Broggini, F., Snieder, R., Wapenaar, K. and Behura, J. [2014] Wave field autofocusing and imaging with multidimensional deconvolution: numerical examples for reflection data with internal multiples. *Geophysics*, **79**, (accepted).
- Fink, M. [2008] Time-reversal acoustics. *Journal of Physics: Conference Series*, **118**, 012001.
- Garnier, J. and Papanicolaou, G. [2014] Role of scattering in virtual source array imaging. *SIAM Journal on Imaging Sciences*, (submitted).
- Slob, E., Wapenaar, K., Broggin, F. and Snieder, R. [2014] Seismic reflector imaging using internal multiples with Marchenko-type equations. *Geophysics*, **79**, (accepted).
- van der Neut, J., Vasconcelos, I. and Wapenaar, K. [2014] An interferometric interpretation of Marchenko Redatuming. *EAGE, Extended Abstracts*, (This conference).
- Virieux, J. and Operto, S. [2009] An overview of full-waveform inversion in exploration geophysics. *Geophysics*, **74**(6), WCC1–WCC26.
- Wapenaar, K., Broggin, F., Slob, E. and Snieder, R. [2013] Three-dimensional single-sided Marchenko inverse scattering, data-driven focusing, Green's function retrieval, and their mutual relations. *Physical Review Letters*, **110**, 084301.
- Wapenaar, K., Thorbecke, J., van der Neut, J., Broggin, F., Slob, E. and Snieder, R. [2014] Marchenko imaging. *Geophysics*, **79**, (accepted).